



Liquefaction of sedimentary rocks during impact crater development



J.P. Hippertt^a, C. Lana^{a,*}, R.F. Weinberg^b, E. Tohver^c, M. Schmieder^c, R. Scholz^a,
L. Gonçalves^a, J.F. Hippertt^d

^a Departamento de Geologia, Universidade Federal de Ouro Preto, Ouro Preto, Minas Gerais, 35400-000, Brazil

^b School of Earth, Atmosphere and Environment, P.O. Box 28E, Monash University, Melbourne, Victoria 3800, Australia

^c School of Earth and Environment, University of Western Australia, 35 Stirling Hwy, Crawley, WA 6009, Australia

^d Instituto de Bio y Geociencias del NOA (IBIGEO), Universidad Nacional de Salta, CONICET, Av. Bolivia 5150, 4400 Salta, Argentina

ARTICLE INFO

Article history:

Received 7 December 2013

Received in revised form 5 September 2014

Accepted 29 September 2014

Available online 31 October 2014

Editor: C. Sotin

Keywords:

impacts

liquefaction

meteorite

Araguainha

sandstone

microbrecciation

ABSTRACT

Impact crater development on every planetary body requires catastrophic movement of large volumes of crustal rocks. The process produces well-known features such as brecciation and frictional melting, but a mechanism that explains how rocks accommodate the strain during the cratering flow remains unclear. Here, we investigate target rocks from the Araguainha impact crater (central Brazil) that typify what happens to a consolidated, fluid-saturated sedimentary rock at ~2 km below the surface prior to the impact event. Sandstone units record a pattern of chaotic large-scale folds and pervasive microscopic (grain-to-grain) brecciation that result from rock strength degradation triggered by the impact. Field mapping and extensive textural observations indicate that these sandstones experienced initial microstructural damage from the shock wave and that this process may have weakened grain-to-grain bonds and started the process of pervasive microbrecciation. Accompanying heating and decompression lead to vaporization and expansion of fluids in the sandstone pores, magnifying the process of brecciation by effectively liquefying the rock mass and allowing for chaotic folding (at a range of scales up to blocks 100 m in length) in the central uplift. This is a vaporization-assisted microbrecciation, and it may have inhibited the formation of pseudotachylites, because energy was dissipated by pervasive microcracking, vaporization of pore fluids, and large scale chaotic folding, rather than localized displacement on brittle faults and frictional heating. We suggest that impact liquefaction of sedimentary rocks depends on whether the presence of pore-fluids and related micro-brecciation are sufficient to dissipate most of the impact energy.

© 2014 Elsevier B.V. All rights reserved.

1. Introduction

The formation of large impact craters involves highly energetic/destructive processes that include rock vaporization, melting and pseudotachylitic brecciation (Melosh, 1989; French, 1998; Ivanov et al., 2010). Shock waves emanating from the collision may reach speeds up to 10 km/s and set rocks into a flow motion to form a bowl-shaped transient cavity within seconds of the collision. For complex craters, the rock flow is highly effective in that the rim of the initial cavity expands kilometers away from the impact point and seconds later it collapses back to form the final crater structure (e.g., Lana et al., 2006). The nature of this process is unknown to any tectonic environment operative on Earth and, consequently, the mechanism that best explains the sudden reduction in rock strength remains obscure. One explanation is that

violent acoustic vibrations could temporarily reduce the internal frictional strength of the rocks, allowing them to behave like fluids (Melosh, 1979; Melosh and Ivanov, 1999). This model is convenient because liquefied debris has an effective viscosity sufficiently low to permit collapse within the required time-scale. Other physical models propose that rocks lose internal cohesion through thermal softening due to extreme temperatures released upon impact (O'Keefe and Ahrens, 1993), but direct evidence for these theoretical models have not been fully documented in nature. While there are many studies of the characteristic effects of shock deformation on target rocks, the phenomenon that causes loss of cohesion in target rocks around large impact structures has not been fully documented. Here we show that the structural integrity of fluid-saturated sedimentary rocks is destroyed at grain scale by shock damage and pore-fluid expansion during the impact.

Large-scale "ductile" fold structures are observed in and around central uplifts of a number of craters including the Spider and Lawn Hill craters in Australia, the Vredefort Dome in South Africa

* Corresponding author. Tel.: +55 31 98483538; fax: +55 31 35591606.

E-mail address: cristianoelclana@gmail.com (C. Lana).

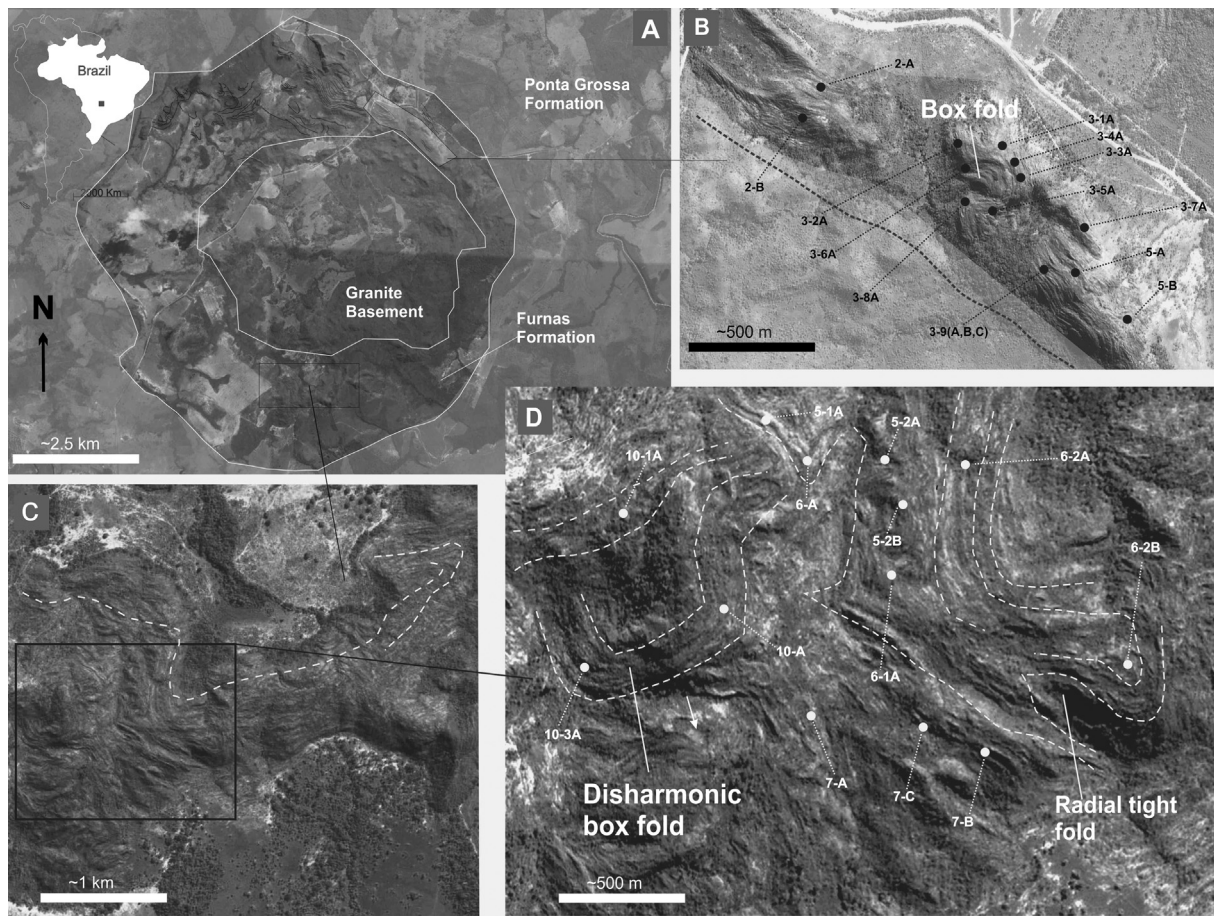


Fig. 1. A: Satellite image of the uplift with the distributions of the different formations marked (the granite core and surrounding Furnas and Ponta Grossa Formations). B: Enlarged image of the northeastern ridge of the central uplift in A. C: Aerial photograph of the southeastern ridge. White dashed line highlights the contorted nature of the bedding at the granite/sandstone contact. D: Enlarged image of southern ridge, depicting km-scale fold geometries in the Furnas Formation. White dashed lines mark the trend of bedding. The numbers are sample localities.

and the Araguainha structure in central Brazil (Lana et al., 2003a, 2004, 2006, 2008; Abels, 2005; Wieland et al., 2005; Salisbury et al., 2008; Tohver et al., 2013). These folds are the best expression of extreme compressional strain recorded in central uplifts of a number of complex craters in sedimentary and mixed (sedimentary+crystalline) target rocks (e.g., Lana et al., 2003a, 2006; Wieland et al., 2005). Their contorted nature seems to require a prodigious change in bulk-rock strength that suggests either ductile or fluid-like behavior. In addition, folded sedimentary strata in and around central uplifts seem to be devoid of pseudotachylite. Pseudotachylites are more commonly described in crystalline rocks of large impact structures (e.g., the Vredefort Dome) whereby the deformation is thought to occur through intense fracturing/faulting and frictional shearing (Melosh, 2005; Spray, 1995, 2010; Lana et al., 2003b, 2004).

In this paper, we focus on the highly contorted sedimentary strata from the 10–12 km-wide central uplift of the 254.7 ± 2.5 Ma Araguainha impact structure (Tohver et al., 2012) in central Brazil (Fig. 1A). The Araguainha central uplift comprises a 5 km-wide granitic core surrounded by a collar of upturned or overturned strata of the Furnas and Passa Dois Formations (e.g., Lana et al., 2007, 2008). The highest intensity of impact-related folding is in the older stratigraphic units (inner collar strata) that have been thickened by a factor of 3 to 5 (Lana et al., 2006, 2008). Thickening is particularly evident for the Devonian sandstone unit of the central uplift (Furnas Formation), which is exceptionally thick to the north, west, and southwest sectors of the core-collar contact (Figs. 1A–D). On the scale of the crater, rocks of the Furnas

Formation comprise 400 m to 800 m wide, fault-bounded blocks of highly folded strata (e.g., Fig. 1B). The blocks themselves are marked by highly contorted fold structures (Figs. 1B–D) and represent an excellent natural laboratory to investigate large-scale flow of target rocks during impact events.

2. Background

The Araguainha structure is located in the northern margin of the Paraná Basin (Lana et al., 2006, 2007, 2008). It is morphologically marked by a 10–12 km diameter central uplift surrounded by a 15–20 km wide annular trough, with two concentric rings and the crater rim (Lana et al., 2007). The central uplift is divided into a 2 km-thick collar of Devonian to Carboniferous clastic sedimentary rocks of the Paraná Basin (Furnas and Ponta Grossa Formations) and a 4 km-wide core of late Cambrian granitic basement (Figs. 1A–D) (Engelhardt et al., 1992; Tohver et al., 2012, 2013). The annular trough exposes Devonian pelites/sandstones of the Ponta Grossa Formation and Carboniferous red sandstones/conglomerates of the Aquidauana Formation.

Elsewhere in the Paraná basin, the Furnas sandstones are known as flat-lying, predominantly undeformed, medium- to coarse-grained, quartzarenite to subarkose sandstones, with 80–90% quartz, 2–10% feldspars and minor accessory minerals. Oil and gas-related studies show that the sandstone porosity ranges from 2 to 15% across the Furnas Formation. Pore connectivity may be limited due to replacement of feldspars and diagenetic precipitation of kaolinite or illite (De Ros, 1998; Melo and Giannini, 2007).

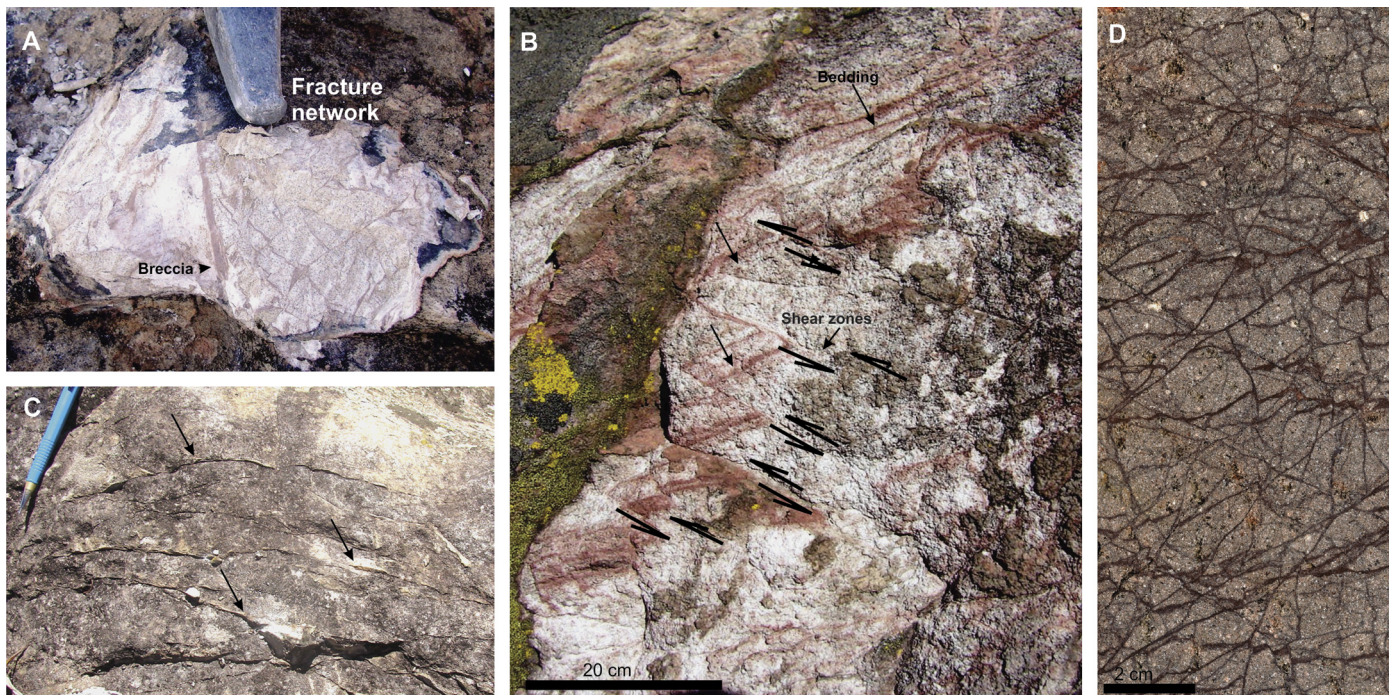


Fig. 2. A: Network of orthogonal fracture systems in the Furnas sandstones. Note the network is bounded by a cm-wide breccia (locality 2A in Fig. 1B). B: Sets of parallel faults that cross-cut sandstone bedding. Spacing between faults is ~ 10 cm (locality 7A in Fig. 1D). C: Irregular fractures filled with matrix (locality 6-2A in Fig. 1D). The groundmass in this case is developed locally and seems to be more resistant to weathering than the sandstone. D: Shocked and sheared sandstone from one of the most intensely tectonized Furnas sandstone blocks, at the eastern flank of the central uplift (1 km north of locality 2A in Fig. 2B).

Micas (1–10%) are common in its fine-grained sandstone and siltstone layers. Previous XRD and SEM analyses indicate that authigenic clays include kaolinite and its polymorph dickite (De Ros, 1998). Pore-filled kaolinite is a characteristic feature (0–44 vol.%; av. 13%) of this formation throughout the basin.

Within the Araguinha impact structure, the Furnas Formation is the most prominent rock unit of the central uplift. The best exposures are found along km-scale ridges, in the northeastern and southeastern sectors of the central uplift (Figs. 1A–C). These ridges comprise a 400 m to 800 m-thick pile of clastic quartzose layers segmented into fault-bounded blocks that are rotated independently, forming a megabreccia zone around the granite core (Lana et al., 2006, 2008).

The basal units within the Furnas Formation at Araguinha consist dominantly of milky-white arkoses and sandstone beds, intercalated with cm- to m-thick, pink to reddish siltstones (e.g., Fig. 2B). The individual mature sandstones layers are medium- to coarse-grained, locally grading into conglomeratic levels (Lana et al., 2007). Some of the intraformational/depositional cycles are capped by micaceous mudstones. Bedding structures are defined by the alternation of 5 to 30 cm-thick quartz-feldspar-rich layers and thin 2 to 5 mm-wide iron-rich lenses (Fig. 2B). The reddish siltstone layers are marked by the alternation between mm-wide, iron oxide-rich and feldspar-rich bands. Most of the feldspar-rich levels are altered and significantly more friable than the other sandstone layers. The contact between the strata of the Furnas Formation and the granite core is obscured by the presence of the overlying crater infill material. Stratigraphic and structural reconstructions of the pre-impact target stratigraphy indicate that this core-collar contact was approximately 2 km below surface, consistent with bore-hole core logging some 100 km north of the impact crater (Engelhardt et al., 1992; Lana et al., 2006, 2007). More recently, Machado et al. (2009) showed field and petrographic observations that this contact was within or substantially close to the zone of impact melting during the cratering event, which explains

the presence of sandstone-derived melt around the central uplift (Engelhardt et al., 1992; this study).

3. Methodology

Field-based structural observations of the Furnas Formation were carried out around the collar of the central uplift. Some 27 block samples (Figs. 1B, C) were made into thin sections for optical and scanning electron microscopy (SEM). Fabric analysis included quantification of grain-shape, modal analysis of clast and matrix via point counting and Arc-GIS based image processing. The ImageJ software (Collins, 2007) was used to refine the textural quantification of grains and matrix in 22 selected samples. Major element analyses of the main phases were carried out using Energy Dispersive Spectroscopy at the Centro de Microscopia – Universidade Federal de Minas Gerais, Brazil.

4. Impact-induced folding

The refolded and disharmonic fold geometries of the Furnas strata in the central uplift describe a complex fabric pattern (Figs. 1A–C; Lana et al., 2008). The most prominent structures are km-scale, radially plunging, open to tight folds in the southeastern and northeastern ridges of the central uplift. Generally, the smooth, gently-curved, bedding orientations are sharply truncated by radial strike-slip fault zones (Lana et al., 2008) that separate km-scale blocks of folded sandstones at different scales (Figs. 1A, B). The presence of classic box folds, ranging from meters to hundreds of meters in scale (Figs. 1B–D), and the radially plunging open to tight folds, are consistent with the radial constriction of the sediments around the core of the central uplift. However, the highly contorted fold geometries make strain analysis around the collar unworkable. The complexity of the fold geometries encompasses highly variable bedding orientations, which dip sub-vertically to vertically in the near vicinity of the crystalline core (see Lana et al., 2006, 2008).

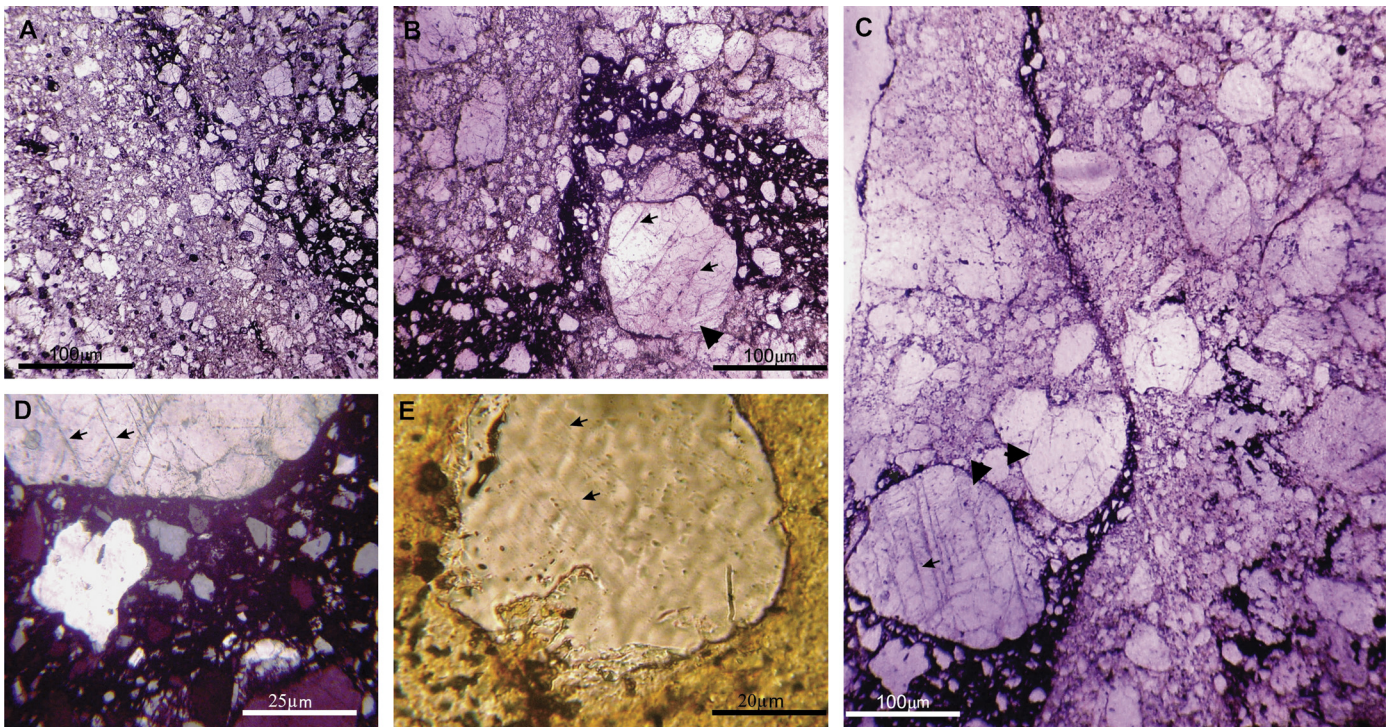


Fig. 3. A: Pervasive brecciation of the Furnas sandstones where most of the original round grains were converted to angular fragments, which are floating in a microcrystalline groundmass. B–C: Portions of the sandstones that partly preserve a few round, pre-impact grains. Note that a few round grains preserve impact related planar features (PF, arrows). D: Contrast between a round grain with decorated PF and surrounding highly angular grains. All grains are supported by groundmass. E: Detail of quartz grain with annealed planar features and corroded boundaries.

At the outcrop scale, all folds are associated with meter-wide, pervasively distributed networks of fractures and less common breccia veins (Fig. 2A). Most outcrops record fractures that are often arranged into various sets (Figs. 2A–C). Individual fractures show curved or planar geometries and are localized around meter-wide fault zones, which disrupt bedding planes in the central uplift. The offset observed across individual fractures is generally small, ranging from 5 to 30 cm (Fig. 2C). Some highly fractured domains feature the localized development of meter-wide shear zones, which can be classified into two different types: 1) bedding-parallel, strike-slip shear zones occurring along pelitic layers; and 2) cataclastic shear zones developed on the coarse-grained beds of the Furnas strata (Lana et al., 2006).

Individual shear zones or fracture planes are filled with a fine-grained reddish groundmass. This material is common along branching fractures planes, locally forming brecciated fracture networks (Figs. 2A–C). Although these clast-bearing fractures are rather rare features, they can reach several meters in length, and are typified by the presence of angular, millimetric quartz fragments embedded in a reddish fine-grained matrix.

5. Microbrecciation

All 27 samples selected from the Furnas sandstones and siltstones (Figs. 1B, D) show pervasive grain-scale fracturing that has complexly obliterated the original sedimentary texture (e.g., Fig. 3A). Such a degree of grain scale fragmentation contrasts with coherent sedimentary features seen at outcrop scale. For instance, while satellite images depict systematic bedding orientations within the individual ridges of the Furnas sandstones (e.g., Fig. 1) (see also Lana et al., 2008), optical microscopy shows a chaotic arrangement of poorly-sorted, angular, shocked and non-shocked quartz grains (Figs. 3A–C). Extensive mapping of the Furnas Formation (e.g., Lana et al., 2006, 2007, 2008; this work) shows

that pervasive brecciation is only observed at the grain scale and is marked by whole-grain and/or grain-boundary fragmentation.

Grains that preserve their pre-impact, round (detrital) shapes are rare (e.g., Figs. 3B, E). Most quartz grains are highly angular (in the form of shards) produced by extreme fragmentation of pre-impact quartz. These angular grains are suspended in a microcrystalline/isotropic groundmass (Figs. 3D, E). In the least brecciated samples, the grains were only comminuted along their edges and rarely preserve grain-to-grain contacts (Fig. 4A). In such cases, the pre-impact textures with intergrain pores are partly preserved. Most of the samples, however, do not record the pre-impact fabric and grain-to-grain bonds have been lost and replaced by a brecciated microstructure (Figs. 4B, C). The grains are either partly or completely fragmented (Figs. 4C, D) in jig-saw fit textures (previously documented by Kieffer, 1971 and Osinski, 2007). For most parts, however, the grain fragments are dislocated and/or rotated from the site of brecciation.

Even the mechanically more resistant minerals are brecciated. For example, Fig. 5 shows shocked and brecciated grains of zircon and monazite (see also Tohver et al., 2012). Monazite may appear partly to completely recrystallized, leaving behind a trail of monazite subgrains in some thin sections (Figs. 5A–C). In fact, dissolution/precipitation of monazite and Fe oxides are common features of the ground mass, and their trails (Figs. 5B, C) suggest substantial fluid flow during or immediately after the impact. In contrast, zircons appear mainly fractured (Fig. 5D). Fragments of zircon appear as trails of angular grains in the groundmass (Fig. 5E). Some of the zircon grains show one and two sets of planar fractures and their grain boundary fragments are offset from the main grain core (Fig. 5F).

It is worth noting that there are some key textural differences between shock metamorphic features and brecciation. For example, brecciated grain fragments commonly lack impact features, whereas one or more sets of planar fractures, as well as annealed and decorated features, may be preserved in pre-impact

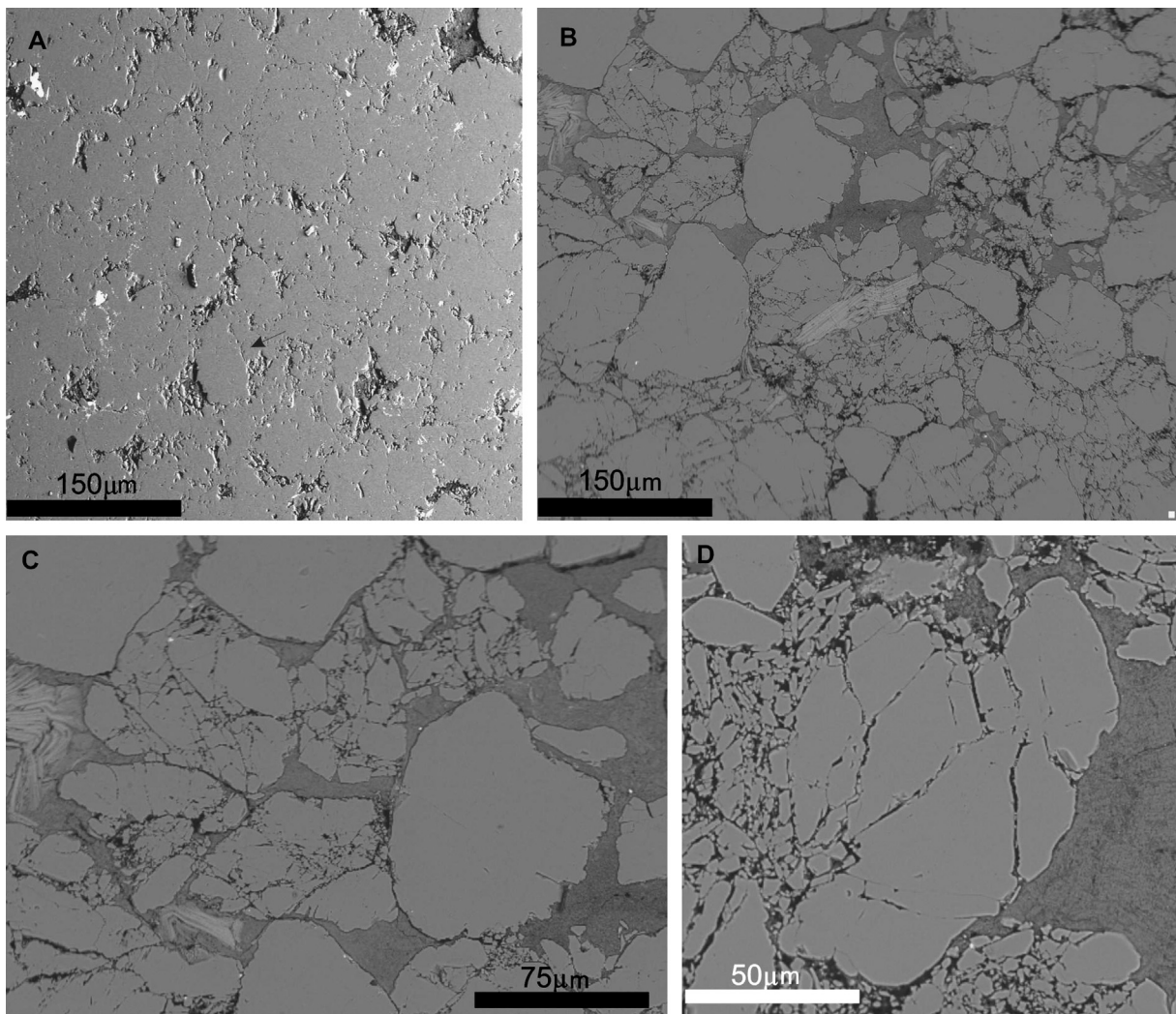


Fig. 4. Scanning electron microscopy images of sandstone samples showing: A: Partly preserved pre-impact textures with intact grain contacts and intergrain pores slightly modified due to grain-to-grain wear. The initial stages of grain boundary abrasion can be inferred by the speckled pattern within darker matrix. Arrow points to preserved grain boundary. B–C: Clast-supported breccia with local development of groundmass. Note some grain shards floating in a structureless groundmass. C: Contrast between round, “preserved” quartz grains and surrounding angular grains (C is a detail of B). D: Individual original grain still in situ but strongly cracked, broken up into small fragments mostly with jigsaw fit. (A: secondary electron image; B–D: backscattered electron images.)

round grains (black arrows in Figs. 3D, E). The planar features are similar to decorated Planar Deformation Features (PDFs) observed in other large complex structures such as the Vredefort Dome (e.g., Reimold and Gibson, 1996). Unlike grains in the original Furnas sandstones, many grains display corroded boundaries, suggestive of disequilibrium reactions between grain fragments and the surrounding matrix or the overheated fluids that might have flowed through the pores immediately after impact. The reaction affected not only the grain boundaries but also the planar features (e.g., Fig. 3E), indicating that the reaction occurred after the shock. In fact, both the microbrecciation and grain-boundary corrosion post-date the shock induced planar features in quartz, zircon and monazite (Figs. 5A–F).

The breccia textures are not evenly distributed but vary significantly across the central uplift. Detailed scanning electron microscopy shows domains of distinctive microstructures generated by the brecciation of similar rock types. For instance, Figs. 4C, D and 5E, F show examples of clast-supported and matrix-supported breccias, respectively. These microstructures are observed in both medium- to fine-grained sandstones and rarely in coarse-grained samples. The main difference between the microstructures is

the volume percentage of groundmass. Fine-grained sandstones and silt layers display mainly matrix-supported breccias and are marked by as much as 65–70% of fragmented quartz, embedded in a microcrystalline Si–Al-rich amorphous groundmass (Fig. 4C). In many medium- to fine-grained samples, quartz grains are literally floating in the groundmass, which encompasses the remaining 30–35% of the bulk composition of the fine-grained sandstones. In domains with lower abundances of fine, fragmented quartz (0.01–0.1 mm), the groundmass can reach up to 35–40% in volume. Medium- and coarse-grained sandstone samples commonly develop into clast-supported breccias (e.g., Figs. 5B, D, E), marked by the highest abundance of small, angular grains (0.01–0.1 mm wide) produced by extreme crushing of larger (rounded) quartz grains.

Figure 6 shows the results of point counting and image analyses of 22 samples from the northern and southern ridges of the collar (see Fig. 1 for sample localities). The samples were arranged, from left to right, according to the intensity of microbrecciation. For instance, samples with the lowest degree of brecciation (left side of the diagram) are the ones with the highest proportion of groundmass (described below). Fine-grained sandstones and siltstones

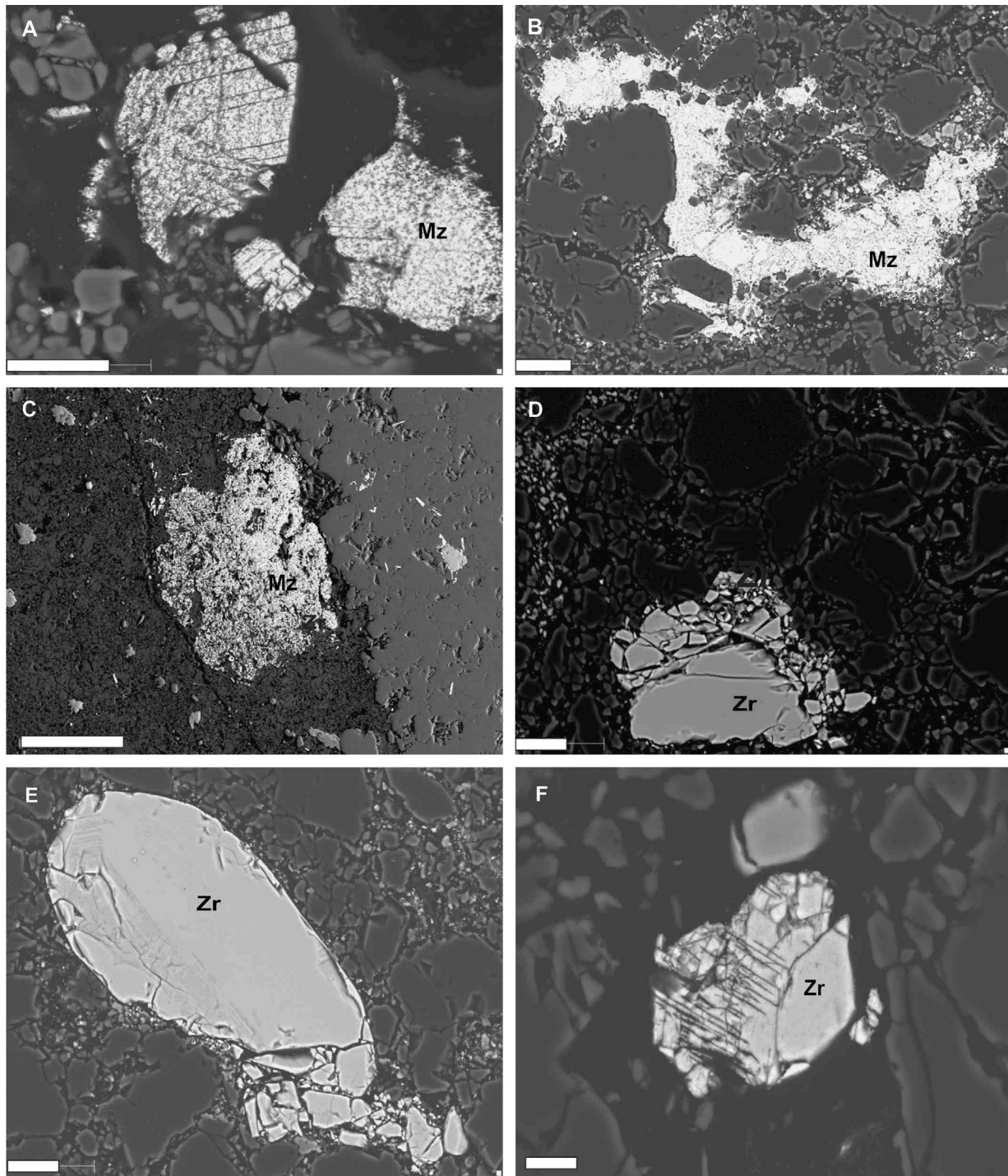


Fig. 5. A–C: Monazite (Mz) partly to completely recrystallized and fragmented. Note that crystals show planar features and that these predate fragmentation. Larger grains in the matrix B–C are partly dissolved and reprecipitated. D–F: Zircon (Zr) grain showing partial fragmentation and planar features. Notice in D how zircon fragments have flowed away from the source grain. E: Intensely broken-up zircon grain in a clast-supported breccia. F: Planar feature in zircon, partly affected by brecciation. White bar is 20 μm .

(samples 3-8A, 5A and 5B) tend to have the highest content of matrix and, consequently, the largest number of preserved pre-impact grains and the lowest number of grains with jigsaw fit textures. In contrast, samples with the lowest matrix content (samples 2A, 7C, 3-5A) show a sharp variation in texture, with the highest percentage of grains showing jigsaw fit and the lowest number of preserved pre-impact clasts. The average grain size is similar across all samples, however, the matrix-rich samples were initially finer-grained (as most preserved pre-impact grains were fine-grained)

whereas the average grain size in the matrix-poor samples is dictated by the amount of impact-related grain fragmentation (micro-brecciation).

6. Shear zone networks

Micro-shear zones are observed in both coarse- and fine-grained sandstone samples but are absent in pelitic samples. The 27 samples collected throughout the Furnas sandstones (Fig. 1)

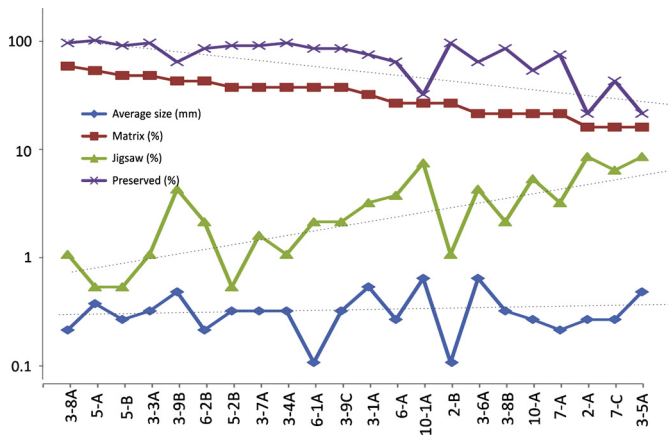


Fig. 6. Results of point counting and image analyses of several samples around the central uplift. Plot shows the area percentage of grains with jigsaw fit, and of preserved grains, determined by their large and rounded shape. X-axis shows sample numbers and sample location is shown in Figs. 1B–D. Preserved percentage refers to percentage of preserved quartz grains in relation to total clast grains whereas matrix percentage is in relation to the total area of the thin section.

show shear zones with well-defined boundaries, and are internally characterized by comminuted grains embedded in an isotropic groundmass (Fig. 7). Micro-shear zones are classified into two main categories, primary and secondary shear zones, according to their relative size.

The primary shear zones are m-long features with widths ranging from 0.1 mm to 5 cm (Figs. 1B; 7A–C). These shear zones occur generally in oblique conjugate sets, with spacing varying between 2 and 10 mm (Figs. 7A, B), but bifurcations are common in highly sheared samples (Fig. 7C). The offset observed for each individual shear zone is small, with a maximum displacement in the order of centimeters. The most prominent feature in these shear zones is the high content of small fragments (0.001–0.05 mm wide), resulting from the intense grain size reduction through cataclasis or wear abrasion (Figs. 7D, E). Fine grains are angular with irregular rims, with the smallest grains being wedge-shaped. The proportion of groundmass is highly variable, generally ranging from 10 to 50% (Figs. 7E, G, H), but in places the shear zone is 90% filled by the groundmass (Fig. 7F).

Secondary shear zones form complex networks of bifurcations, shooting off from primary shear zones (Figs. 7A, C). They complete the pervasive network of shear/fracture surfaces, generally in the domains between adjacent, parallel to subparallel primary shear zones. Such secondary shear zones are mm-sized and are irregular, marked by intense grain-size reduction (e.g., pulverized quartz). Some samples of the Furnas sandstone collected at the eastern flank of the central uplift collar, where a block of the reddened sandstone is in contact with siltstones and also juxtaposed by impact melt rock, show an intricate 3D network of dark shear bands on the cm-scale (Fig. 2D). In such domains, the sandstone appears to have been transformed into a tectonic breccia, with a number of intersecting dark shear bands apparently oriented at random; locally, reddish pelitic units are preserved as angular slivers between and within the shear bands. Like for the aforementioned larger-scale primary and secondary shear zones in the Furnas sandstone collar, the network of shear bands is composed of a particulate matrix and mineral grains floating therein, indicating cataclastic flow mechanisms but no incipient melting of the host sandstone along mm- to cm-scaled slip planes.

7. Groundmass

Fine-grained groundmass forms the matrix of the brecciated sandstone. This ground mass is observed in micro-shear zones,

fractures and forms mm-scale patches around shattered quartz (Figs. 8A, B). This groundmass is found in all brecciated samples of the Furnas Formation and consists of an isotropic yellow material, in which angular quartz fragments are suspended (Figs. 3E and 8C). Flow texture within the groundmass is highlighted by trails of Fe-oxides (Figs. 8A, B). Both optical and scanning electron images indicate that the groundmass in the matrix and in the shear zones share identical textural homogeneity, similar in many ways to an impact glass phase (e.g., cooled from an impact melt). However typical impact-melt quench textures suggestive of fast cooling (e.g., Machado et al., 2009) have not been observed. Detailed SEM images show instead that it consist of submicroscopic clay minerals (predominantly kaolinite and allophane) with a dominant Si–Al-rich composition and minor amounts (<1%) of K, Fe. The presence of kaolinite seems to be a common feature of Furnas sandstones in most parts of the Paraná Basin (De Ros, 1998).

Well-developed microcrystals of kaolinite are observed in all thin sections (Figs. 8D, E), particularly in more micaceous layers of the Furnas sequence, where the groundmass represents more than 40% of the sample. Reactive textures represented by corrosion/resorption, observed in quartz and feldspar crystals in direct contact with the groundmass (Fig. 3E), suggest disequilibrium textures generated by fluid activity within the pervasive fracture network of the brecciated samples. Particularly large (pre-impact) quartz grains are marked by corroded boundaries (Figs. 8C, D) that provide evidence of chemical disequilibrium between the fluidized matrix and the brecciated fragments. Corrosion along fractures in quartz is generally accompanied by arrays of both fluid and solid inclusions (Fig. 8F). Large muscovite grains also show reaction textures along grain boundaries. Large feldspar grains may show corrosion textures as well, with pervasive embayments and symplectitic intergrowths absent from similar grains from undeformed Furnas sandstones (Fig. 8G). Feldspar grains are generally surrounded by larger volumes of groundmass than elsewhere. In contrast, fine-grained sericite aggregates do not show any reaction textures and are interpreted to have formed as secondary alteration minerals of the groundmass.

8. Sandstone-derived melt rock

Rare patches of black to varicolored, fluidal, and strongly silicic (>85% SiO₂) impact melt rocks occur overlying the Furnas sandstones, near the impact breccia exposures in the northern sector of the dome (see also Engelhardt et al., 1992; Lana et al., 2007). Optical and SEM images show that these impact melt rocks consist of a fine-grained polycrystalline, schlieren-rich, fluidal groundmass of intergrown silica and feldspar, as well as micrometer-sized idiomorphic flakes of melt-crystallized Fe–Ti oxides. Inherited elongated sandstone clasts and larger mineral grains are intensely flow-banded, aligned along the main direction of melt flow, locally arranged in an ‘imbrication’ pattern, and mainly composed of recrystallized quartz (Figs. 9A–C). The melt rock contains abundant granular zircon (Wittmann et al., 2006; Timms et al., 2012) mostly with preserved rounded, detrital mineral grain outlines and relict shock metamorphic features (Fig. 9D).

9. Discussion

9.1. Liquefaction of sandstones

Impact cratering is a highly energetic process involving intensive, rapid flow of enormous rock volumes. Within the Araguinha impact structure, this flow pattern generated chaotic folds in sandstone. The issue is that for most impact craters, large segments of sedimentary strata, such as in the Araguinha central uplift and other large impact craters (e.g., Spider and Lawn Hill in

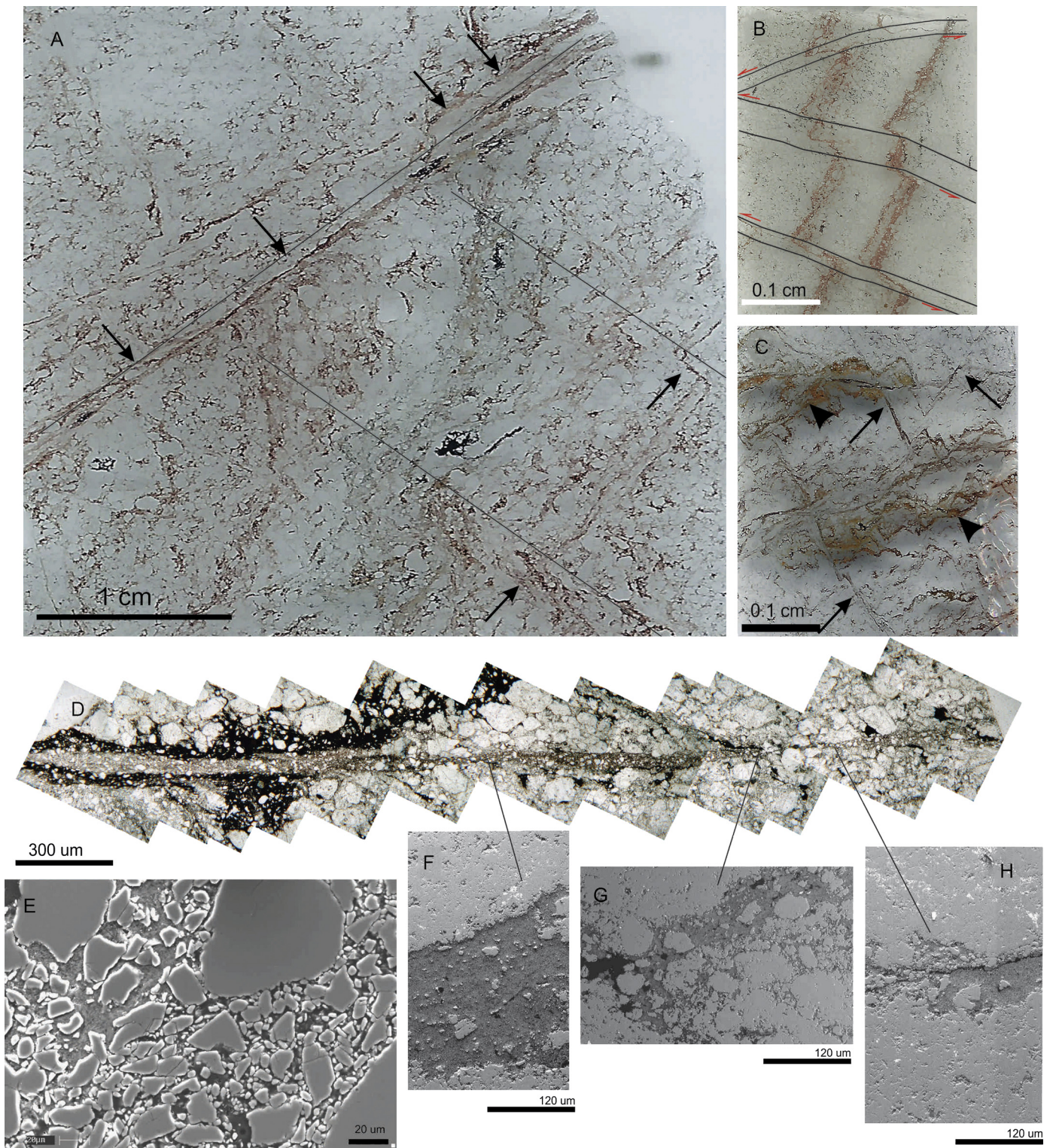


Fig. 7. Sets of shear zones observed in thin sections. A–C: Scanned thin sections showing shear zones displacing bedding. Note that primary shear zones are generally straight (main shear zone in A, whereas secondary shear zones are irregular and less prominent (as in B), see text for details). C: Conjugate sets of orthogonal shear zones (black arrows) crosscutting highly brecciated bedding planes (arrow heads). Note that the shear bands post-date brecciation. D: Photomicrograph mosaic of shear zone across a thin section. Shear zone is irregular on a micro-scale and overall they are marked by irregular clasts floating in a groundmass. E–H: Scanning electron microscopy, backscattered electron images detailing shear zone in D. Shear zone walls vary from irregular to sharp and record intense grain size reduction through cataclasis or wear abrasion.

Australia; Abels, 2005; Salisbury et al., 2008; Vredefort in South Africa; Wieland et al., 2005; Lana et al., 2003a, 2003b, 2008) describe rather smooth and continuous fold geometries, which are consistent with a viscous rock deformation. Outcrop, petrography and modeling all suggest that at least part of the large-scale

folding in sedimentary strata is accompanied by intense brittle fracturing (Nicolaysen and Reimold, 1999; Collins et al., 2004; Grieve et al., 2008), faulting and block rotation (Wieland et al., 2005; Grieve et al., 2008; Lana et al., 2008). Likewise, previous microstructural studies of a cm-wide impact fold from the

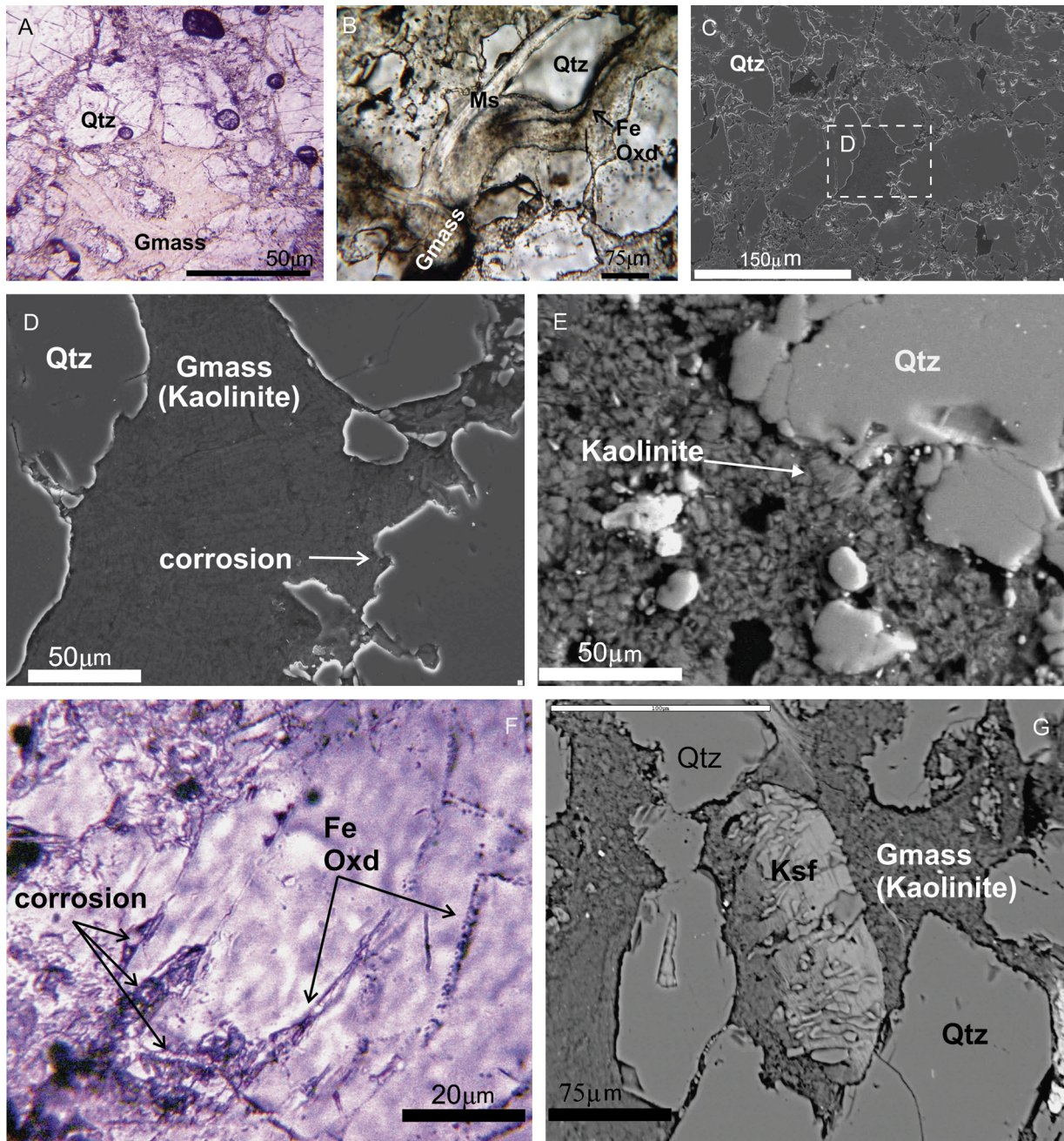


Fig. 8. The groundmass (Gmass) and groundmass-reaction features in the Furnas sandstones. A: Photomicrograph (plane polarized light) showing yellowish groundmass patch surrounded by quartz (Qtz) grains. B: Photomicrograph (plane polarized light) of groundmass surrounding muscovite (Ms). Note that groundmass in both A and B record flow textures highlighted by trails of Fe-oxides. C, D: Scanning electron microscopy image of groundmass patch surrounded by fragments of highly corroded quartz (Qtz). Note that the groundmass is formed by submicroscopic crystals of kaolinite. E: Scanning electron microscopy image of well-developed kaolinite in groundmass. F: Photomicrograph showing corrosion along fractures in quartz generally accompanied by arrays of both fluid and solid inclusions. G: Partly corroded grain of K-feldspar (Kfs) and corroded grains of quartz (Qtz) embedded in groundmass. K-feldspar is typically characterized by symplectitic textures shown by the small wormy quartz grains.

7 km-wide Crooked Creek impact crater in Missouri (USA), suggest that the viscous rock behavior is achieved by localized brittle deformation along millimeter- to centimeter-spaced fault zones (Kenkmann, 2002). Kenkmann (2002) attributed localized brittle deformation during folding to a reduction of internal cohesion due to shock damage. At Araguinha, complex folding takes place at a scale of hundreds of meters to kilometers and affected the entire sandstone sequence of the Furnas Formation around the central uplift. Thus, the question is how did the rocks lose internal cohesion on that scale to allow complex folding without major faulting or widespread macroscopic brecciation.

Similarly to the small-scale folds in the Crooked Creek crater, the Araguinha folds lack evidence for folding in the ductile regime where rocks are folded as the result of intracrystalline deformation. Figs. 5 to 8 show instead that these impact folds resulted from a loss of cohesion due to pervasive microbrecciation. The presence of decorated PDFs and intense fluid inclusions in the shocked grains suggests that this grain-scale brecciation was triggered by the shock wave (causing initial shock damage) and by heating and expansion of pore fluids into vapor.

The base of the Furnas sandstones was at an estimated 2 km depth prior to the impact (Lana et al., 2007). Assuming an average

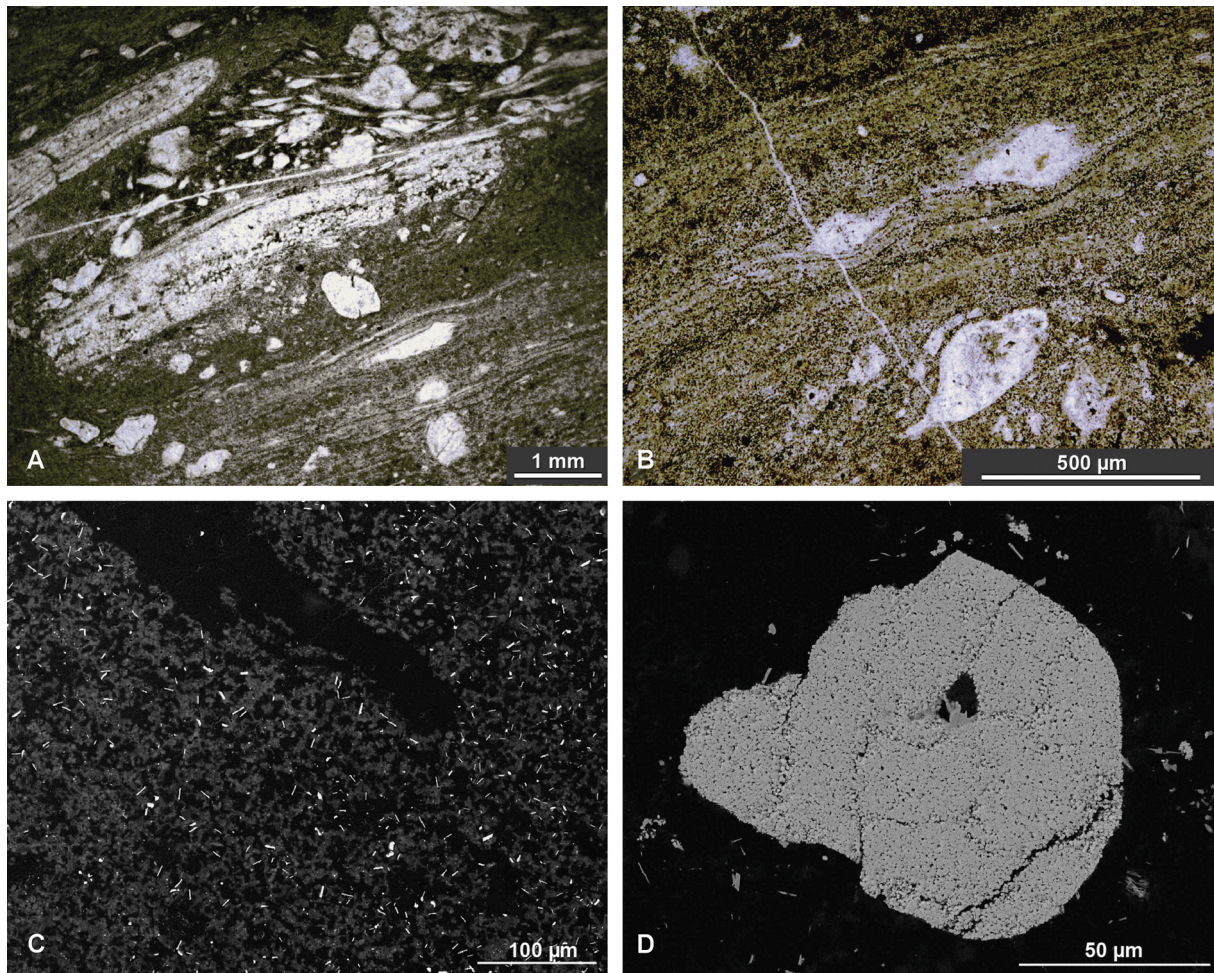


Fig. 9. Sandstone-derived impact melt breccia from the central Araguainha impact structure. A: Overall fabric of the rock with partially melted fluidal sandstone clasts and larger quartz grains floating within a fluidal melt matrix. B: Close-up of fluidal melt domain with patches of recrystallized silica (A and B plane-polarized light). C: Backscattered electron image showing melt matrix composed of an intergrowth of feldspar, silica, and Fe-Ti oxides, and elongated clast of melted quartz at the top. D: Granular detrital zircon with rounded grain outline in the melt rock (backscattered electron image).

crustal density of 2800 kg/m^3 , we can infer a pre-impact (lithostatic) pressure in the range of 0.50–0.55 kbar across the Furnas Formation. Thus, the slightest increase in pressure and temperature driven by the impact would change fluid pressure conditions in pores of the Furnas sandstones, lowering yield strength of the rock. In addition, the highly folded sandstone units were close to the impact melt zone where temperatures were sufficiently high ($>1000^\circ\text{C}$) to cause melting of the sandstones (Fig. 9), boiling of pore-fluids and induce intense fluid circulation in sediments (Fig. 8). We suggest that brecciation may have been caused by three mechanisms working simultaneously: (1) initial shock damage, (2) fluid expansion caused by vaporization due to heating and decompression, leading to pressurization of the pores, breaking grain-to-grain contacts, and (3) melting in regions of temperature maxima. At the moment of impact, the sandstone would fail through intense micro-fracturing, and boiling would partly buffer the maximum temperatures reached during dissipation of shock wave energy. This vapor-enhanced pervasive brecciation could thus explain the effective liquefaction of these rocks and the origin of large-scale chaotic folds.

Hydrothermal fluid circulation (e.g., Osinski and Pierazzo, 2012) may have persisted while the system cooled and fluids subsequently escaped through porous flow and along the multiple shear zones (Figs. 3, 7). This explains intense circulation of fluids in the Furnas sandstones as highlighted by: (1) corrosion features in quartz (Fig. 3E), (2) monazite dissolution/precipitation features

(Fig. 5B), and (3) Fe-Ti oxides precipitation along the planar features in quartz (Fig. 8F).

Soil or sediment liquefaction occurs when saturated or partially saturated sediments substantially lose strength and stiffness in response to an applied, oscillating stress (Casagrande, 1976; Jefferies and Been, 2006). Essentially this phenomenon is linked to the passage of compressive and rarefactive waves such as earthquake shaking or other abrupt change in stress conditions, causing it to behave like a liquid. The primary weakening of the Araguainha target rocks was caused by pervasive shock damage and fluid expansion (e.g., Figs. 4 to 8), and the fragmented quartz grains were kept initially in a pressurized vapor, gradually compacting as the system cooled, vapor condensed and hydrothermal fluids precipitated the matrix material. Thus, chaotic folding of the sandstone around the central uplift may have been largely dependent on the presence of fluid in a porous rock.

9.2. Pore-fluid expansion, sandstone microbrecciation, and the absence of pseudotachylites

Pseudotachylites, as the products of frictional melting, seem to be exceptionally rare in porous sandstones at terrestrial impact structures. Only in very rare instances and in connection with the largest impact structure on Earth have pseudotachylitic breccias been reported, e.g., in the Hospital Hill Quartzite (a weakly metamorphosed sandstone that has lost most of its initial porosity)

at the giant Vredefort impact structure in South Africa (Reimold and Gibson, 1996). Similarly, siliciclastic rocks have rarely developed pseudotachylites in deformation experiments (e.g., Logan et al., 1973; Friedman et al., 1974) but tend towards brittle failure and subsequent cataclastic deformation in response to high stress and strain rates (e.g., Wong et al., 1997). The lack of extensive shear zones or fractures filled with pseudotachylites in the Furnas sandstone, such as found in the granitic core of the Araguinha central uplift (Machado et al., 2009), is a result of their very different responses to the impact. In the sandstones, impact energy was dissipated by pervasive microbrecciation, associated with heating, boiling and expansion of pore fluids, microbrecciation and creation of the incohesive, liquefied mass. This process prevented the sandstone from behaving as large rigid blocks, incapacitating the generation of frictional melts on large, localized fault planes.

We conclude that the combination of microbrecciation, cataclasis and fluid expansion due to vaporization gave rise to an effectively unconsolidated rock. This explains the large-scale folding of the Furnas sandstone strata around the central uplift (Fig. 1) within the short time scale of an impact event (seconds/minutes) and the absence of pseudotachylites.

Acknowledgements

This research was funded by FAPEMIG (PROJECT APQ 0870/11) and the Australian Research Council (DP110104818) to Weinberg. J.P. Hippertt acknowledges scholarship from FAPEMIG (PROBIC – Process 9/2012). The paper benefited from constructive reviews from Editor Christophe Sotin and two anonymous reviewers.

References

- Abels, A., 2005. Spider impact structure, Kimberley Plateau, Western Australia: interpretations of formation mechanism and age based on integrated map-scale data. *Aust. J. Earth Sci.* 52, 653–664.
- Casagrande, A., 1976. Liquefaction and Cyclic Deformation of Sand – A Critical Review. *Harvard Soil Mechanics Series*, vol. 88. Harvard University, Cambridge. 27 pp.
- Collins, T.J., 2007. ImageJ for microscopy. *BioTechniques* 43 (1 Suppl.), 25–30.
- Collins, G.S., Melosh, H.J., Ivanov, B.A., 2004. Modeling damage and deformation in impact simulations. *Meteorit. Planet. Sci.* 39, 217–231.
- De Ros, L.F., 1998. Heterogeneous generation and evolution of diagenetic quartzarenites in the Silurian–Devonian Furnas Formation of the Paraná Basin, southern Brazil. *Sediment. Geol.* 116 (1–2), 99–128.
- Engelhardt, W., Matthai, S., Walzebeck, J., 1992. Araguinha impact crater, Brazil. I: the interior part of the uplift. *Meteorit. Planet. Sci.* 27, 442–457.
- French, B.M., 1998. *Traces of Catastrophe: Handbook of Shock-Metamorphic Effects in Terrestrial Meteorite Impact Structures*. Lunar and Planet. Institute, Houston. 120 pp.
- Friedman, M., Logan, J.M., Rigert, J.A., 1974. Glass-indurated quartz gouge in sliding-friction experiments on sandstone. *Geol. Soc. Am. Bull.* 85, 937–942.
- Grieve, R.A.F., Reimold, W.U., Morgan, J., Riller, U., Pilkington, M., 2008. Observations and interpretations at Vredefort, Sudbury, and Chicxulub: towards an empirical model of terrestrial impact basin formation. *Meteorit. Planet. Sci.* 43, 855–882.
- Ivanov, B.A., Melosh, H.J., Pierazzo, E., 2010. Basin-forming impacts: reconnaissance modeling, in large meteorite impacts. *Spec. Pap., Geol. Soc. Am.* 465, 29–49.
- Jefferies, M.G., Been, K., 2006. *Soil Liquefaction – A Critical State Approach*. Taylor & Francis, ISBN 0-419-16170-8. 478 pp.
- Kenkmann, T., 2002. Folding within seconds. *Geology* 30, 231–234.
- Kieffer, S.W., 1971. Shock metamorphism of the Coconino Sandstone at Meteor Crater, Arizona. *J. Geophys. Res.* 76, 5449–5473.
- Lana, C., Filho, C.R.S., Marangoni, Y.R., Yokoyama, E., Trindade, R.I.F., Tohver, E., Reimold, W.U., 2008. Structural evolution of the 40 km wide Araguinha impact structure, central Brazil. *Meteorit. Planet. Sci.* 43 (4), 701–716.
- Lana, C., Gibson, R.L., Reimold, W.U., 2003a. Impact tectonics in the core of the Vredefort dome, South Africa: implications for central uplift formation in very large impact structures. *Meteorit. Planet. Sci.* 38, 1093–1107.
- Lana, C., Gibson, R.L., Reimold, W.U., 2003b. Archean crustal structure of the Kaapvaal craton, South Africa – evidence from the Vredefort dome. *Earth Planet. Sci. Lett.* 206, 133–144.
- Lana, C., Gibson, R.L., Reimold, W.U., 2004. Pseudotachylite-fracture network: a key structure for central uplift formation in large impact structures meteorit. *Planet. Sci. Suppl.* 39, 5062.
- Lana, C., Romano, R., Reimold, W.U., Hippertt, J.F., 2006. Collapse of large complex impact structures: implications from the Araguinha impact structure. *Geology* 34, 9–12.
- Lana, C., Souza-Filho, C., Marangon, I.Y., Yokoyama, E., Trindade, R., Tohver, E., Reimold, W.U., 2007. Insights into the morphology, geometry and post-impact erosion of the Araguinha peak-ring structure, central Brazil. *Geol. Soc. Am. Bull.* 119, 1135–1150.
- Logan, J.M., Iwasaki, T., Friedman, M., Kling, S.A., 1973. Experimental investigation of sliding friction in multilithologic specimens. In: Pincus, H. (Ed.), *Geological Factors on Rapid Excavation*. In: *Geol. Soc. Am., Eng. Geol.*, vol. 9, pp. 55–67.
- Machado, R., Lana, C., Stevens, G., Reimold, W.U., McDonald, I., 2009. Generation, mobilization and crystallization of impact-induced alkali-rich melts in granitic target rocks: evidence from the Araguinha impact structure, central Brazil. *Geochim. Cosmochim. Acta* 73, 7183–7201.
- Melo, M.S., Giannini, P.C.F., 2007. Sandstone dissolution landforms in the Furnas Formation, southern Brazil. *Earth Surf. Process. Landf.* 32, 2149–2164.
- Melosh, H.J., 1979. Acoustic fluidization: a new geologic process? *J. Geophys. Res.* 84 (7), 513–7520.
- Melosh, H.J., 1989. *Impact Cratering – a Geological Process*. Oxford University Press. 245 pp.
- Melosh, H.J., 2005. The mechanics of pseudotachylite formation in impact events. In: Koeberl, C., Henkel, H. (Eds.), *Impact Tectonics*. In: *Impact Studies*, vol. 6. Springer, Heidelberg, pp. 55–80.
- Melosh, H.J., Ivanov, B.A., 1999. Impact crater collapse. *Annu. Rev. Earth Planet. Sci.* 27, 385–415.
- Nicolaysen, L.O., Reimold, W.U., 1999. Vredefort shatter cones revisited. *J. Geophys. Res.* 104 (B3), 4911–4930.
- O’Keefe, J.D., Ahrens, T.J., 1993. Planetary cratering mechanics. *J. Geophys. Res.* 98, 17011–17028.
- Osinski, G.R., 2007. Impact metamorphism of CaCO₃-bearing sandstones at the Houghton structure, Canada. *Meteorit. Planet. Sci.* 42 (11), 1945–1960.
- Osinski, G.R., Pierazzo, E., 2012. *Impact Cratering: Processes and Products*. Wiley–Blackwell. 330 pp.
- Reimold, W.U., Gibson, R.L., 1996. Geology and evolution of the Vredefort impact structure, South Africa. *J. Afr. Earth Sci.* 23, 125–162.
- Salisbury, J.A., Tomkins, A.G., Schaefer, B.F., 2008. New insights into the size and timing of the Lawn Hill impact structure: relationship to the Century Zn–Pb deposit. *Aust. J. Earth Sci.* 55 (4), 587–603.
- Spray, J.G., 1995. Pseudotachylite controversy: fact or friction? *Geology* 23, 1001–1004.
- Spray, J.G., 2010. Frictional melting processes in planetary materials: from hypervelocity impact to earthquakes. *Annu. Rev. Earth Planet. Sci.* 38, 221–254.
- Timms, N.E., Reddy, S.M., Healy, D., Nemchin, A.A., Grange, M.L., Pidgeon, R.T., Hart, R., 2012. Resolution of impact-related microstructures in lunar zircon: a shock-deformation mechanism map. *Meteorit. Planet. Sci.* 47, 120–141.
- Tohver, E., Cawood, P.A., Riccomini, C., Lana, C., Trindade, R.I.F., 2013. Shaking a methane fizz: seismicity from the Araguinha impact event and the Permian–Triassic global carbon isotope record. *Palaeogeogr. Palaeoclimatol. Palaeoecol.* 387, 66–75.
- Tohver, E., Lana, C., Cawood, P.A., Fletcher, I.R., Jourdan, F., Sherlock, S., Rasmussen, B., Trindade, R.I.F., Yokoyama, E., Souza Filho, C.R., Marangoni, Y., 2012. Geochronological constraints on the age of a Permo–Triassic impact event: U–Pb and ⁴⁰Ar/³⁹Ar results for the 40 km Araguinha structure of central Brazil. *Geochim. Cosmochim. Acta* 86, 214–227.
- Wieland, F., Gibson, R.L., Reimold, W.U., 2005. Structural analysis of the collar of the Vredefort Dome, South Africa – significance for impact-related deformation and central uplift formation. *Meteorit. Planet. Sci.* 40, 1537–1554.
- Wittmann, A., Kenkmann, T., Schmitt, R.T., Stöffler, D., 2006. Shock-metamorphosed zircon in terrestrial impact craters. *Meteorit. Planet. Sci.* 41, 433–454.
- Wong, T.F., David, C., Zhu, W., 1997. The transition from brittle faulting to cataclastic flow in porous sandstones: mechanical deformation. *J. Geophys. Res.* 102, 3009–3025.